[15] Lindeberg, T., ter Haar Romeny, B. M.: Linear scale-space: (I) Basic theory and (II) Early visual operations. In: Geometry-Driven Diffusion. (ter Haar Romeny, ed.), pp. 1–77, Kluwer Academic Publishers/Springer, Dordrecht, Netherlands (1994).
[16] Lorenz, D. A., Bredies, K., Zeevi, Y. Y.: Nonlinear complex and cross diffusion. Unpublished report, University of Bremen, 2006.
[17] Pauwels, E. J., Van Gool, L. J., Fiddelaers, P., Moons, T.: An extended class of scale-invariant and recursive scale space filters. IEEE Trans. Pattern Analysis and Machine Intelligence. 17(7), 691-701 (1995).
[18] Pazy, A.: Semigroups of Linear Operators and Applications to Partial Differential equations, Springer, New York (1983).
[19] Perona, P., Malik, J.: Scale–space and edge detection using anisotropic diffusion. IEEE Trans. on Pattern Anal. and Mach. Intell. 12 629–639 (1990).
[20] Weickert, J.: Anisotropic Diffusion in Image Processing. B.G. Teubner, Stuttgart (1998).
[21] Weickert, J., Ishikawa, S., Imiya, A.: On the History of Gaussian Scale-Space Axiomatics. In: Gaussian Scale-Space Theory, J. Sporring, M. Nielsen, L. Florack, P. Johansen (Eds), Computational Imaging and Vision (vol. 8), Springer Science+Business Media Dordrecht (1997). Originally published by Kluwer Academic Publishers in 1997.
[22] Witkin, A. P.: Scale-space filtering. Proc. Eighth Int. Joint Conf. on Artificial Intelligence (IJCAI'83), Vol. 2, pp. 1019-1022, Karlsruhe (1983).
[23] Yuille, A. KL., Poggio, T. A.: Scaling theorems for zero crossings. IEEE Trans. on Pattern Analysis and Machine Intelligence. 8, 15–25 (1986).
[24] Yosida, K.: Functional Analysis, Springer, Berlin (1995).

Adérito Araújo
CMUC, Department of Mathematics, University of Coimbra, Portugal
E-mail address: alma@mat.uc.pt

Sílvia Barbeiro
CMUC, Department of Mathematics, University of Coimbra, Portugal
E-mail address: silvia@mat.uc.pt

Eduardo Cuesta
Department of Applied Mathematics, University of Valladolid, Spain
E-mail address: eduardo@mat.uva.es

Ángel Durán
Department of Applied Mathematics, University of Valladolid, Spain
E-mail address: angel@mac.uva.es

Pré-Publicações do Departamento de Matemática
Universidade de Coimbra
Preprint Number 16–22

CROSS-DIFFUSION SYSTEMS FOR IMAGE PROCESSING: I. THE LINEAR CASE

ADÉRITO ARAÚJO, SÍLVIA BARBEIRO, EDUARDO CUESTA AND ÁNGEL DURÁN

Abstract: The use of cross-diffusion systems as mathematical models of different image processes is investigated. The present paper is concerned with linear filtering. First, those systems satisfying the most important scale-space properties are identified. Then a numerical study on the effect of cross-diffusion in filtering problems is presented.

1. Introduction

This paper takes part of a study on the application of cross-diffusion systems in image processing. It is devoted to linear filtering and will be continued by a second part concerning the nonlinear case.

The most common representation of a grey-scale image is given by a real valued function $u = u(\mathbf{x}) \in L^1(\mathbb{R}^2)$ (that is in the space of integrable functions on the plane) where $u(\mathbf{x}) = u(x, y)$ stands for the grey-scale value of the image at the pixel at position $\mathbf{x} = (x, y)^T$, [2, 12, 20]. The introduction, from u, of two scalar fields may have the goal of distributing the features of the image and governing the relations among them.

The use of cross-diffusion models is widespread in disciplines like, for instance, population dynamics, (see [7, 8] and references therein) while their application to image processing is to our knowledge less common. In this sense, two references are relevant for us and motivate this and the subsequent work. The first one is the so-called complex diffusion, [11]. Here the original, real image evolves according to a complex diffusion process which implies some sharing out of the information between the real and the imaginary parts of the complex function representing the image. The effect of this division has been analyzed in [9, 10, 11]. In particular, the linear case reveals the key role of the imaginary part as edge detector, since it behaves as a smoothed Laplacian scaled by time when the phase angle of the complex diffusion coefficient is small (the so-called small theta approximation). This also motivates the extension of complex diffusion to nonlinear models.

Received May 20, 2016.

Complex diffusion can indeed be rewritten as a cross-diffusion model for the real and imaginary parts of the image function. This is used in the second reference, [16], to analyze the existence of global solution of a related cross-diffusion system and to compare this with Perona-Malik models, [19], by computational means. In addition to the theoretical advantage of having a global solution, the computational study shows a better performance of the proposed cross-diffusion system.

The present paper aims to go deeply into this approach. Focused on the linear case, when features of the image are distributed in two components $\mathbf{u} = (u, v)^T$, the most general linear filtering will involve a matrix convolution

$$K * \mathbf{u}(\mathbf{x}) = \begin{pmatrix} k_{11} * u(\mathbf{x}) + k_{12} * v(\mathbf{x}) \\ k_{21} * u(\mathbf{x}) + k_{22} * v(\mathbf{x}) \end{pmatrix}, \tag{1.1}$$

where

$$K = \begin{pmatrix} k_{11} & k_{12} \\ k_{21} & k_{22} \end{pmatrix},$$

is the matrix kernel. The entries k_{ij} can be chosen to control the filtering process according to the information provided by each component of $\mathbf{u}$ as well as other theoretical properties of the restoration. According to this, the main contribution of the paper is two-fold:

- By defining the linear filtering processes in form of matrices convolutions, those kernels satisfying the scale-space properties of recursivity, grey-level shift, rotational and scale invariance are characterized. This generalizes previous results for the scalar case, [17].
- We provide a computational study of the linear filters according, essentially, to the choice of the initial data (that is, the way how the information of the initial image is distributed) and on some parameters of the convolution kernels. Our numerical experiments on one- and two-dimensional signal restoration problems seek to reveal the flexibility of the models and the performance through the computation of some indexes to measure the quality of restoration.

The structure of the paper is as follows. In Section 2 the matrix convolution (1.1) is formulated as a linear cross-diffusion model and some scale-space properties are analyzed. Under some hypotheses, those kernels are characterized in terms of the cross-diffusion matrix. A generalized version of the

according to the results, a relevant degree of adaptability which enables them as an alternative for linear filtering.

The present paper will be continued in a natural way by the introduction of nonlinear cross-diffusion models and the study of their behaviour in image restoration.

5. Acknowledgments

This work was supported by Spanish Ministerio de Economía y Competitividad under the Research Grant MTM2014-54710-P. A. Araújo and S. Barbeiro were also supported by the Centre for Mathematics of the University of Coimbra – UID/MAT/00324/2013, funded by the Portuguese Government through FCT/MCTES and co-funded by the European Regional Development Fund through the Partnership Agreement PT2020.

References

[1] Álvarez, L., Guichard, F., Lions, P.-L., Morel, J.-M.: Axioms and fundamental equations for image processing. Arch. Rational Mech. Anal. 123, 199–257 (1993).
[2] Aubert, J., Kornprobst, P.: Mathematical Problems in Image Processing, Springer-Verlag, Berlin (2001).
[3] Babaud, J., Witkin, A. P., Baudin, M., Duda, R. O.: Uniqueness of the Gaussian kernel for scale-space filtering. IEEE Trans. Pattern Analysis and Machine Intelligence. 8, 26–33 (1986).
[4] Brezis, H.: Functional Analysis, Sobolev Spaces and Partial Differential Equations, Springer, New York (2011).
[5] Canuto, C., Hussaini, M. Y., Quarteroni, A., Zang, A. T.: Spectral Methods in Fluid Dynamics, Springer, New York (1985).
[6] Florack, L. M. J., ter Haar Romeny, B. M., Koenderink, J. J., Viergever, M. A.: Scale and the differential structure of images. Image and Vision Computing. 10, 376–388 (1992).
[7] Galiano, G., Garzón, M. J., Jüngel, A.: Analysis and numerical solution of a nonlinear cross-diffusion system arising in population dynamics. Rev. R. Acad. Cie. Ser. A Mat. 95(2), 281–295 (2001).
[8] Galiano, G., Garzón, M. J., Jüngel, A.: Semi-discretization in time and numerical convergence of solutions of a nonlinear cross-diffusion population model. Numer. Math. 93, 655–673 (2003).
[9] Gilboa, G., Zeevi, Y. Y., Sochen, N. A.: Complex diffusion processes for image filtering. In: Scale-space and Morphology in Computer Vision, pp. 299-307, Springer, Berlin (2001).
[10] Gilboa, G., Sochen, N. A., Zeevi, Y. Y.: Generalized shock filters and complex diffusion. In: Computer Vision-ECCV, pp. 399-413, Springer, Berlin (2002).
[11] Gilboa, G., Sochen, N. A., Zeevi, Y. Y.: Image enhancement and denoising by complex diffusion processes, IEEE Trans. Pattern Analysis and Machine Intelligence. 26(8), 1020–1036 (2004).
[12] Guichard, F., Morel, J. M.: Image Analysis and P.D.E.'s. IPAM GBM Tutorials, 2001.
[13] Lindeberg, T.: Scale-space for discrete signals. IEEE Transaction on Pattern Analysis and Machine Intelligence. 12, 234-254 (1990).
[14] Lindeberg, T.: Scale Space. In: Encyclopedia of Computer Science and Engineering (B. Wah ed.), Vol IV, pp. 2495–2509, John Willey and Sons, Hoboken New Jersey (2009).

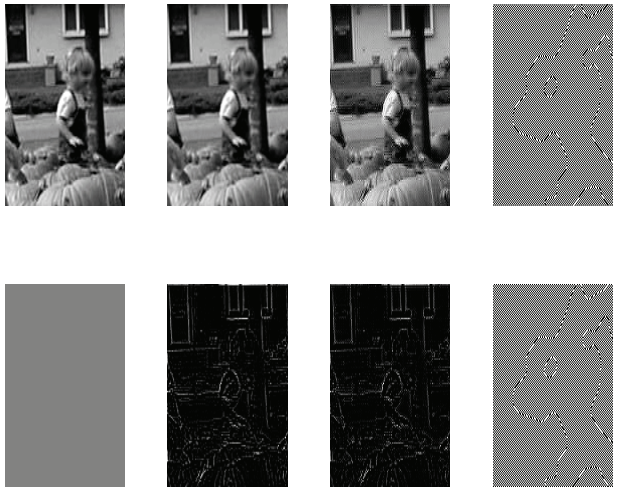

FIGURE 20. Cross-diffusion with $p = 2$ and for $\theta = 10\pi/30$ ($\mu \approx 1.732051$). Evolution of components u (top) and v (bottom) at times $t_* = 0, 0.25, 2.5, 25$ with d_4.

is positive definite (observe the final image in Figure 20) this cross-diffusion case gives the best correlation coefficient with the original image.

4. Conclusions and perspectives

In the present paper linear cross-diffusion systems for image processing are analyzed. Viewed as convolution processes, those kernels satisfying fundamental scale-space properties are characterized, generalizing the results presented in the literature for the scalar case, [15]. This generalization is also extended to the property of small theta approximation, introduced in the case of the linear complex diffusion, [11], which is identified in terms of the entries of the corresponding matrix convolution.

In a second part, a numerical study of comparison with kernels is made. The numerical experiments, performed for one- and two-dimensional signals, show the influence of the choice of the initial distribution of the image in a vector of two components, as well as of the matrix of the kernel on the behaviour of the restoration process by cross-diffusion. The models present,

small theta approximation property (that is, the identification of a component of the image as edge detector) is also studied. Section 3 is devoted to some experiments of comparison among the models characterized in Section 2. Using one- and two-dimensional signals, the comparison is focused on the influence of the parameters presented in the models and on the corresponding goodness of filtering. Finally, the main conclusions and perspectives are outlined in Section 4. The present paper will be followed by a second one, on the inclusion of nonlinearity in the cross-diffusion models.

2. Linear cross-diffusion filtering

The linear filtering (1.1) can be formulated into a scaling process with a family of convolution operators $\{\mathcal{K}_t, t \geq 0\}$ such that

$$\mathbf{u}(\mathbf{x}, t) = \mathcal{K}_t \mathbf{u}_0(\mathbf{x}) = K_t * \mathbf{u}_0(\mathbf{x}), \tag{2.1}$$

where from an original image $\mathbf{u}_0(\mathbf{x}) = (u_0(\mathbf{x}), v_0(\mathbf{x}))^T$, $\mathbf{u}(\mathbf{x}, t)$ stands for the grey-level value image at pixel $\mathbf{x} \in \mathbb{R}^2$ at the scale t. In (2.1), $K_t = (k_{ij}(\cdot, t))_{i,j=1}^2$ is a 2×2 matrix with convolution entries k_{ij} such that if $\mathbf{u} = (u, v)^T$ then (2.1) can be written as

$$\begin{aligned} u(\mathbf{x}, t) &= k_{11}(\cdot, t) * u_0(\mathbf{x}) + k_{12}(\cdot, t) * v_0(\mathbf{x}), \\ v(\mathbf{x}, t) &= k_{21}(\cdot, t) * u_0(\mathbf{x}) + k_{22}(\cdot, t) * v_0(\mathbf{x}). \end{aligned} \tag{2.2}$$

It is known, [18, 24] that under certain conditions (2.1) admits an equivalent formulation as the initial-value problem

$$\begin{aligned} \mathbf{u}_t(\mathbf{x}, t) &= D\mathbf{u}(\mathbf{x}, t), \quad t > 0, \quad \mathbf{x} \in \mathbb{R}^2, \\ \mathbf{u}(\mathbf{x}, 0) &= \mathbf{u}_0(\mathbf{x}), \end{aligned} \tag{2.3}$$

for some operator matrix D or infinitesimal generator

$$D\mathbf{f} = \lim_{h \to 0^+} \frac{K_h \mathbf{f} - \mathbf{f}}{h}. \tag{2.4}$$

If $D = (D_{ij})_{i,j=1}^2$, system (2.3) can be written in terms of the Fourier symbols $\widehat{D}_{ij}(\xi), i, j = 1, 2$, as the evolution problem

$$\begin{aligned} \frac{d}{dt} \begin{pmatrix} \widehat{u}(\xi, t) \\ \widehat{v}(\xi, t) \end{pmatrix} &= \begin{pmatrix} \widehat{D}_{11}(\xi) & \widehat{D}_{12}(\xi) \\ \widehat{D}_{21}(\xi) & \widehat{D}_{22}(\xi) \end{pmatrix} \begin{pmatrix} \widehat{u}(\xi, t) \\ \widehat{v}(\xi, t) \end{pmatrix}, \\ & \xi \in \mathbb{R}^2, \quad t > 0, \quad \mathbf{u} = (u, v)^T, \end{aligned}$$

with $\widehat{u}(\xi,0)=\widehat{u}_0(\xi),\widehat{v}(\xi,0)=\widehat{v}_0(\xi)$. Thus, formally,

$$\widehat{K}(\xi,t)=e^{t\widehat{D}(\xi)}, \tag{2.5}$$

where $\widehat{K}_t(\xi):=\widehat{K}(\xi,t)$ stands for the 2×2 matrix with entries $\widehat{k}_{ij}(\xi,t), i,j=1,2$. The form of the kernels that is suitable for image processing can be discussed by using the scale-space properties as a guide, in a similar way to what is done in some other references for linear filters, [1, 15, 17, 21]. The gradual satisfaction of scale-space properties for (2.1) will specify the types of operators D in (2.3). In this sense, the conclusions will be similar to those of other references, [17], extending these results to the case of cross-diffusion systems. Because of their relevance in the discussion below, two examples will be shown now. The first one is the linear complex filtering and the second one is a generalization of it in the form of a linear cross-diffusion system.

Example 1. *The linear complex diffusion filtering has the form*

$$\begin{aligned} u_t(\mathbf{x},t) &= \alpha\Delta u(\mathbf{x},t), \quad t>0, \quad \mathbf{x}\in\mathbb{R}^2,\\ u(\mathbf{x},0) &= u_0(\mathbf{x}), \end{aligned} \tag{2.6}$$

where $\alpha=\alpha_R+i\alpha_I$ and with Δ the Laplace operator. The solution $u=u_R+iu_I$ of the initial-value problem for (2.6) is, [11]

$$\begin{aligned} &u(\mathbf{x},t)=H_{\sigma(t),\beta(t)}*u_0(\mathbf{x}),\\ &\sigma(t)=\sqrt{\alpha_R t}, \quad \beta(t)=\alpha_I t, \end{aligned} \tag{2.7}$$

which requires $\alpha_R>0,\alpha_I\in\mathbb{R}$ and, for an image $f=f(\mathbf{x})$, with

$$(H_{\sigma,\beta}*f)(\mathbf{x})=\int_{\mathbb{R}^2}H_{\sigma,\beta}(\mathbf{x}-\mathbf{y})f(\mathbf{y})d\mathbf{y},$$

where $\mathbf{x}=(x,y)$ and for $\sigma>0,\beta\neq 0$

$$\begin{aligned} &H_{\sigma,\beta}=G_\sigma * K_\beta,\\ &G_\sigma(\mathbf{x})=\frac{1}{2\pi\sigma^2}e^{-\frac{|\mathbf{x}|^2}{2\sigma^2}}, \quad K_\beta(\mathbf{x})=\frac{1}{4\pi i\beta}e^{i\frac{|\mathbf{x}|^2}{4\beta}}. \end{aligned}$$

If we take $|\alpha|=1$ then the fundamental solution (2.7) can be rewritten in the form displayed in [11] *for the two dimensional case. As a cross-diffusion system for $\mathbf{u}=(u_R,u_I)^T$, (2.6) can be written as (2.3) with*

$$D=\begin{pmatrix}\alpha_R & -\alpha_I\\ \alpha_I & \alpha_R\end{pmatrix}\begin{pmatrix}\Delta & 0\\ 0 & \Delta\end{pmatrix}. \tag{2.8}$$

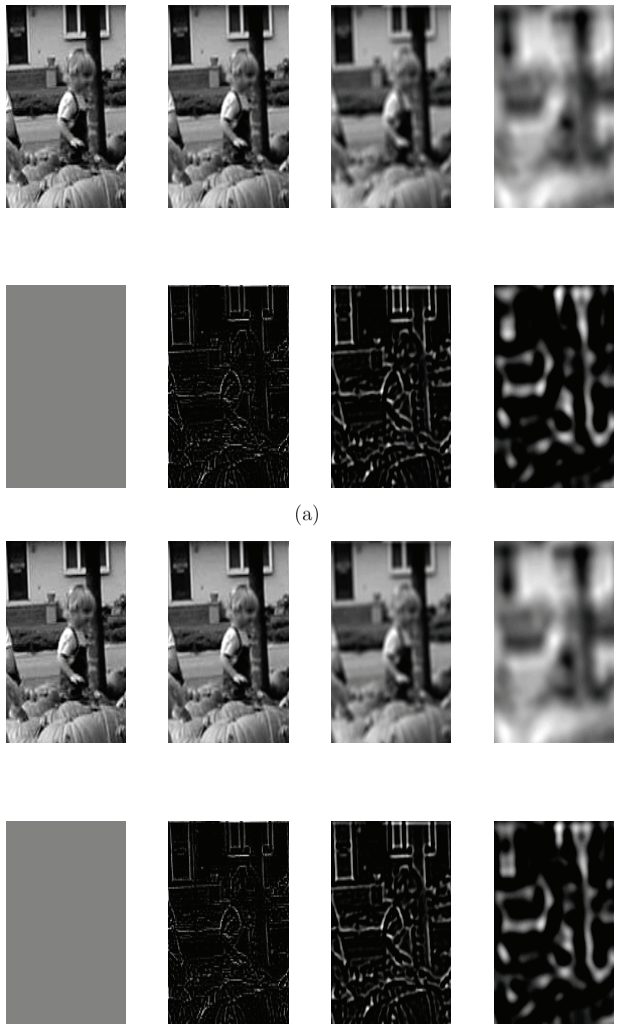

(a)

(b)

FIGURE 19. Cross-diffusion with $p=2$ and for $\theta=10\pi/30$ ($\mu\approx 1.732051$). Evolution of components u (top) and v (bottom) at times $t_*=0,0.25,2.5,25$. (a) d_2 (complex diffusion); (b) d_3.

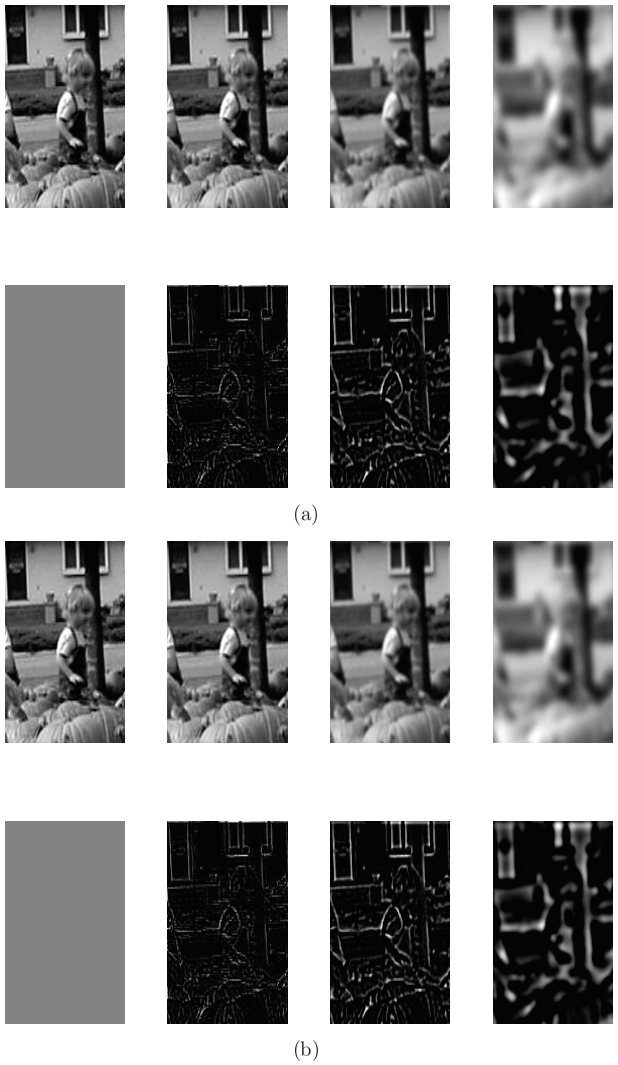

(a)

(b)

FIGURE 18. Cross-diffusion with $p = 2$ and for $\theta = \pi/30$ ($\mu \approx 1.051042E{-}1$). Evolution of components u (top) and v (bottom) at times $t_* = 0, 0.25, 2.5, 25$. (a) d_3; (b) d_4.

Example 2. *The second example can be considered as a generalization of (2.6) with a model of the form (2.3) where*

$$D = \begin{pmatrix} d_{11} & d_{12} \\ d_{21} & d_{22} \end{pmatrix} \begin{pmatrix} \Delta & 0 \\ 0 & \Delta \end{pmatrix},$$

for some 2×2 real matrix $d = (d_{ij})_{i,j=1}^2$. In this case (2.5) is of the form

$$\widehat{K}(\xi, t) = e^{-t|\xi|^2 d}.$$

We will assume that d is positive definite, but not necessarily symmetric. (This means that $\mathbf{x}^T d\mathbf{x} > 0$ for all $\mathbf{x} \neq 0$ or, equivalently, if the symmetric part $(d + d^T)/2$ is positive definite.) This implies that the real part of each eigenvalue is positive. In terms of the entries of d, positive definite character requires two conditions

$$d_{11} > 0, \quad 4d_{11}d_{22} - (d_{12} + d_{21})^2 > 0, \tag{2.9}$$

or equivalently, being

$$\lambda_\pm = \frac{1}{2}\left(d_{11} + d_{22} \pm \sqrt{(d_{11} - d_{22})^2 + 4d_{12}d_{21}}\right), \tag{2.10}$$

the eigenvalues of d, then $Re(\lambda_\pm) > 0$. This may provide several possibilities to choose the matrix d. A particular case consists of matrices of the form

$$d = \begin{pmatrix} \nu & -\mu_1 \\ \mu_2 & \nu \end{pmatrix},$$

with $\nu > 0, \mu_1, \mu_2 > 0, |\mu_1 - \mu_2| < 2\nu$. The case $\mu_1 = \mu_2 := \mu$ corresponds to the linear complex filtering with $\alpha = \nu + i\mu$.

2.1. Scale-space properties. The image representation (2.1) can be interpreted as a scale-space, [1, 13, 14, 15, 21, 20, 22], and its structure in this sense will be analyzed below.

2.1.1. *Grey-level-shift invariance.* We assume that the matrix kernel $K(\cdot, t)$ is mass-preserving. In this context, this means $\widehat{K}(\mathbf{0}, t) = I$ where I is the 2×2 identity matrix; in terms of the entries, we have

$$\begin{aligned} \widehat{k}_{ii}(\mathbf{0}, t) &= \int_{\mathbb{R}^2} k_{ii}(\mathbf{x}, t) d\mathbf{x} = 1, \quad i = 1, 2, \\ \widehat{k}_{ij}(\mathbf{0}, t) &= \int_{\mathbb{R}^2} k_{ij}(\mathbf{x}, t) d\mathbf{x} = 0, \quad i \neq j. \end{aligned} \tag{2.11}$$

Then it looks clear that the filter K_t will not change constant signals:

$$K_t * (\mathbf{f} + \mathbf{C}) = K_t * \mathbf{f} + \mathbf{C}, \quad \mathbf{C} \in \mathbb{R}^2.$$

Conditions (2.11) can also be used to study the preservation by cross-diffusion of some quantities that may be relevant in terms of the image. For $\mathbf{u} = (u, v)^T$ we consider the vector

$$\mathbf{M}(\mathbf{u}) = (m(u), m(v))^T, \;\; m(u) = \left(\int_{\mathbb{R}^2} u(\mathbf{x}) d\mathbf{x} \right). \tag{2.12}$$

Note that for any $f \in L^1(\mathbb{R}^2)$ and $i, j = 1, 2$

$$\begin{aligned} \int_{\mathbb{R}^2} \left(k_{ij}(\cdot, t) * f \right)(\mathbf{x}) d\mathbf{x} &= \int_{\mathbb{R}^2} \int_{\mathbb{R}^2} k_{ij}(\mathbf{x} - \mathbf{y}, t) f(\mathbf{y}) d\mathbf{y} d\mathbf{x} \\ &= \int_{\mathbb{R}^2} \left(\int_{\mathbb{R}^2} k_{ij}(\mathbf{x} - \mathbf{y}, t) d\mathbf{x} \right) f(\mathbf{y}) d\mathbf{y} \\ &= \left(\int_{\mathbb{R}^2} k_{ij}(\mathbf{x}, t) d\mathbf{x} \right) \left(\int_{\mathbb{R}^2} f(\mathbf{x}) d\mathbf{x} \right). \end{aligned}$$

Then, (2.2) and (2.11) imply the preservation of (2.12) by cross-diffusion evolution

$$\mathbf{M}(\mathbf{u}(\cdot, t)) = \mathbf{M}(\mathbf{u}_0), \quad t \geq 0, \tag{2.13}$$

that is $m(u(t)) = m(u_0), m(v(t)) = m(v_0), t \geq 0$. Some consequences of (2.13), in terms of the image processing, can be derived from the choice of the initial data $\mathbf{u}_0$. For example:

(i) If we start from a real image f and make any distribution $\mathbf{u}_0(f) = (u_0(f), v_0(f))$ of grey-level values from it, we may define the average grey-level as $m(u_0) + m(v_0)$ and (2.13) implies the property of average grey-level invariance by cross-diffusion. This includes the particular case of $u_0 = f, v_0 = 0$ (the usual choice in complex diffusion).

(ii) The application of (2.13) may go further the case (i). This depends on the potential meaning of the components of the initial data $\mathbf{u}_0$.

2.1.2. *Rotational invariance.* As in [17] the invariance of the image by rotation is obtained if the kernels only depend on $|\mathbf{x}| = \sqrt{x^2 + y^2}$:

$$k_{ij}(\mathbf{x}) = \kappa_{ij}(|\mathbf{x}|), \quad i, j = 1, 2, \tag{2.14}$$

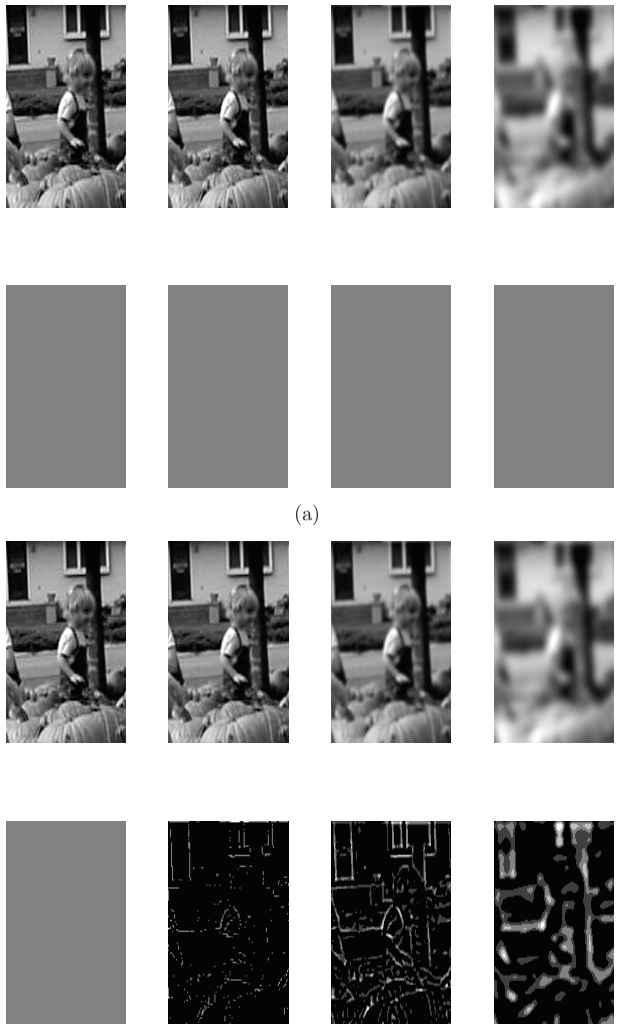

FIGURE 17. Cross-diffusion with $p = 2$ and for $\theta = \pi/30$ ($\mu \approx 1.051042E{-}1$). Evolution of components u (top) and v (bottom) at times $t_* = 0, 0.25, 2.5, 25$. (a) d_1 (Gaussian smoothing); (b) d_2 (complex diffusion).

TABLE 3. Correlation coefficient (2.33) for $\theta = \pi/30$ ($\mu \approx 1.051042E{-}1$).

t	0.25	2.5	25
d_1	$9.993763E{-}1$	$9.839088E{-}1$	$9.205253E{-}1$
d_2	$9.993746E{-}1$	$9.838169E{-}1$	$9.202350E{-}1$
d_3	$9.993602E{-}1$	$9.830421E{-}1$	$9.178705E{-}1$
d_4	$9.993921E{-}1$	$9.847935E{-}1$	$9.234387E{-}1$

TABLE 4. Correlation coefficient (2.33) for $\theta = 7\pi/30$ ($\mu \approx 9.004040E{-}1$).

t	0.25	2.5	25
d_2	$9.992472E{-}1$	$9.776378E{-}1$	$9.043447E{-}1$
d_3	$9.992323E{-}1$	$9.769974E{-}1$	$9.029858E{-}1$
d_4	$9.995045E{-}1$	$9.920391E{-}1$	$9.662403E{-}1$

TABLE 5. Correlation coefficient (2.33) for $\theta = 10\pi/30$ ($\mu \approx 1.732051$).

t	0.25	2.5	25
d_2	$9.988481E{-}1$	$9.643425E{-}1$	$8.812152E{-}1$
d_3	$9.990874E{-}1$	$9.714847E{-}1$	$8.925748E{-}1$
d_4	$9.996072E{-}1$	$9.901388E{-}1$	$1.162159E{-}3$

we have used $\mu = \tan(\theta)$, for $\theta = \pi/30, 7\pi/30, 10\pi/30$, leading to the approximate values of $\mu = 1.051042 \times 10^{-1}, 9.004040 \times 10^{-1}, 1.732051$. It is worth noticing that for the last μ, d_4 fails to be positive definite. The corresponding values of the correlation coefficient (3.3) at several times $t_* = 0.25, 2.5, 25$ for the three cases of μ and the four matrices are given in Tables 3-5. (d_1 does not depend on μ, thus it gives the same results in the three tables.) The evolution of the blurring effect is illustrated in Figures 17-20, which display the two components u, v of $\mathbf{u}$ at t_*.

For the case $\theta = \pi/30$ (small μ) Gaussian smoothing and complex diffusion give very similar correlation coefficient. The results are a little worse for d_2 and d_3 (although the cross-diffusion model incorporates the small theta approximation, as in the complex diffusion case d_2, see the evolution of v in the figures) and better in the case of d_4. As θ increases (larger μ) this behaviour persists; compared to Gaussian smoothing, linear complex diffusion and cross-diffusion with d_3 get worse and worse results, while as long as d_4

for some function κ_{ij}. In terms of the Fourier transform, (2.14) implies that $\widehat{k}_{ij}(\xi), i, j = 1, 2$, can be expressed as

$$\widehat{k}_{ij}(\xi) = \widetilde{\kappa}_{ij}(|\xi|) = \int_0^\infty \kappa_{ij}(\rho) J_0(\rho|\xi|) d\rho, \tag{2.15}$$

where $J_0(z)$ is the zeroth order Bessel function, see [17]. Property (2.14) is verified by the explicit form of $\widehat{K}_t$ in Example 2.

2.1.3. *Regularity and flat kernel as $t \to \infty$.* In order to assume some regularity hypotheses on the operators in (2.1), the literature for the scalar case may serve as inspiration, [1, 3, 6, 15, 17, 23] . In these references, the conditions are diverse and somehow depend on the requirements for the rest of the scale-space properties. According to this, here we may assume the following conditions:

(H1) Required by the semi-group property (see section 2.1.4) we will need $\mathcal{K}_0 = Id$ (the identity operator), that is $K_0 = I$ the 2×2 identity matrix. In terms of the entries of K_t we have $k_{ii}(\cdot, 0) = 1, i = 1, 2$ (or $k_{ii}(\cdot, t)$ tends to Dirac's delta distribution as $t \to 0^+$, [23, 21]) while if $i \neq j$, $k_{ij}(\cdot, 0) = 0$ (or $k_{ij}(\cdot, t) \to 0$ as $t \to 0^+$).

(H2) In order to investigate specific forms of the kernels satisfying the most natural scale-space properties, we assume, as in [17], that each $k_{ij}(\cdot, t) \in L^1(\mathbb{R}^2)$ (the space of integrable functions in $\mathbb{R}^2$) and is separately continuous in $\mathbf{x}$ and t.

(H3) Furthermore, for similar reasons as in (H2) (in particular for the linear complex filtering case) we may follow [3] to assume that each $k_{ij}(\cdot, t)$ is rapidly decreasing in $|\mathbf{x}|$, vanishing at infinity faster than any power of $|\mathbf{x}|$.

Observe that mass preserving property (2.11) is actually a regularity requirement. In particular, it implies flat kernels as $t \to \infty$, that is

$$\lim_{t \to \infty} k_{ij}(\cdot, t) = 0, \quad i, j = 1, 2. \tag{2.16}$$

For the meaning of (2.16) in terms of the image, see [21]. Note also that (H1)-(H3) will be satisfied by the kernels of Example 2 (and therefore, the one of Example 1).

2.1.4. *Recursivity (Semi-group property).* We analyze here the form of the matrices K_t to have the semi-group property

$$\mathcal{K}_0 = Id, \quad \mathcal{K}_{t+s} = \mathcal{K}_t \mathcal{K}_s, \quad t, s \geq 0,$$

that is

$$K_0 = I, \quad K_{t+s} = K_t * K_s, \quad t, s \geq 0, \tag{2.17}$$

where the convolution of two matrices $A = (a_{ij})_{i,j=1}^n$ and $B = (b_{ij})_{i,j=1}^n$ is defined as $C = A * B = (c_{ij})_{i,j=1}^n$ where

$$c_{ij} = \sum_{k=1}^{n} a_{ik} * b_{kj}, \quad i, j = 1, \ldots, n.$$

Note that as in [17] and in terms of the Fourier symbols, condition (2.17) can be written as

$$\widehat{K}_{t+s}(\xi) = \widehat{K}_t(\xi)\widehat{K}_s(\xi), \quad t, s \geq 0, \xi \in \mathbb{R}^2. \tag{2.18}$$

The functional characterization in the matrix case shows that $\widehat{K}_t$ must be of the form (2.5) for some matrix $\widehat{D}$ with $\widehat{D}(\xi) = \widehat{D}(|\xi|)$, see (2.15). (For simplicity the same notation $\widehat{D}$ is used.) Since $k_{ij}(\cdot, t) \in L^1(\mathbb{R}^2)$ then $\widehat{k}_{ij}(\cdot, t) \in C_0(\mathbb{R}^2)$ (the space of continuous functions vanishing at infinity); therefore $\widehat{D}(\xi)$ is continuous and

$$\widehat{D}(\xi) \to -\infty, \quad |\xi| \to \infty.$$

Some other conditions on $\widehat{D}$ will be required to have regularity properties of the resulting semi-group. This will be studied when treating the infinitesimal generator in Section 2.1.6.

2.1.5. *Scale invariance.* The arguments of some references, [15, 17], can be reviewed here to study the scale invariance property. This means, [1], that if $D_\lambda \mathbf{f}(\mathbf{x}) = \mathbf{f}(\lambda \mathbf{x})$ then for any λ and t there is $t' = \phi(t)$ such that

$$D_\lambda K_{\phi(t)} = K_t D_\lambda.$$

We introduce a scale parameter σ, related to the semigroup parameter t by a transformation

$$t = \varphi(\sigma). \tag{2.19}$$

In [15] it is argued that in the context of image processing the relation between t and the scale represented by the standard deviation σ in the Gaussian

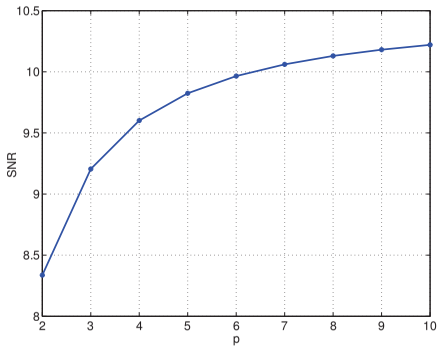

(a)

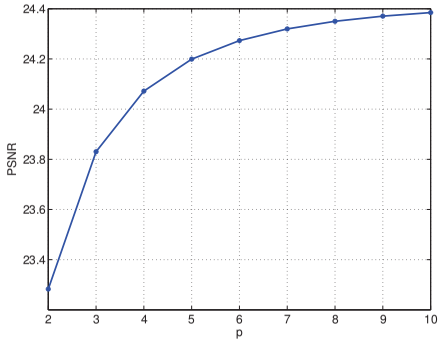

(b)

FIGURE 16. (a) SNR vs. t and (b) $PSNR$ vs. p for a filter (2.1) at $t_* = 2$ with $\mathbf{u}_0^{(1)} = (f, 0)^T$ where f is the initial noisy image affected by additive Gaussian white noise with $\sigma = 30$.

Note that d_1 corresponds to Gaussian smoothing, d_2 represents linear complex diffusion filtering with $c = \nu + i\mu, \nu, \mu > 0$, while matrices d_3 and d_4 are other examples of cross-diffusion, where in d_3 $\nu, \mu > 0, \mu \neq 1$ and in d_4 $\nu, \mu > 0$. In the experiments and for simplicity we fix $\nu = 1$, while the values of μ have been taken in connection with the values of θ considered in [11] (although $c = \nu + i\mu$ does not necessarily have modulus equals one). Thus

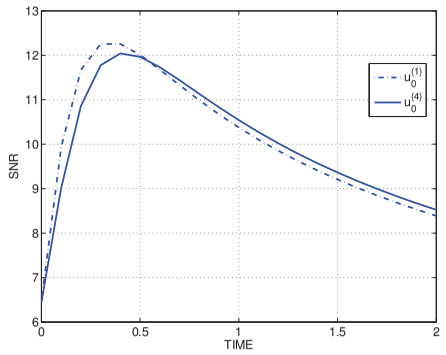

(a)

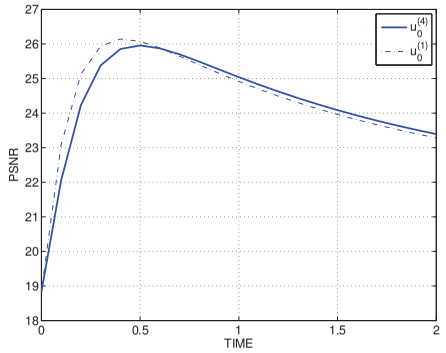

(b)

FIGURE 15. (a) SNR vs. t_* and (b) $PSNR$ vs. t_* for a filter (2.1) with $\mathbf{u}_0^{(1)} = (f, 0)^T$ (solid line) and $\mathbf{u}_0^{(4)} = (f, -|\nabla f|\Delta f)^T$ (dashed line) where f is a noisy image affected by additive Gaussian white noise with $\sigma = 30$.

where $\bar{S}, \bar{U}$ are uniform images with intensities given by the average of intensities of S and U respectively. The matrices for the comparisons are:

$$d_1 = \begin{pmatrix} \nu & 0 \\ 0 & \nu \end{pmatrix}, \quad d_2 = \begin{pmatrix} \nu & -\mu \\ \mu & \nu \end{pmatrix},$$
$$d_3 = \begin{pmatrix} \nu & -\mu \\ 1 & \nu \end{pmatrix}, \quad d_4 = \begin{pmatrix} \nu & \mu \\ 1 & \nu \end{pmatrix}.$$

filtering ($t = \sigma^2/2$) can be generalized and assumed to exist from the beginning of the process, by establishing the existence of time (t) and scale (σ) parameters and some connection (φ) between them. The semigroup condition in terms of σ now reads

$$K(\cdot, \sigma_1) * K(\cdot, \sigma_2) = K(\cdot, \varphi^{-1}(\varphi(\sigma_1) + \varphi(\sigma_2))). \tag{2.20}$$

Condition $K(\cdot, 0) = I$ implies $\varphi(0) = 0$ and in order to preserve the qualitative requirement (which is one of the bases of the scale-space theory, [14]) that increasing values of the scale parameter should correspond to a representation of the image at coarser scales, we must assume that $\varphi : \mathbb{R}_+ \to \mathbb{R}_+$ is monotonically increasing (in particular, invertible). (In [17] this φ can be identified as ψ^{-1} defined there.)

We now adapt the theory of [15] to the linear cross-diffusion filtering through the following steps. Assume that in terms of the scale σ, (2.1) is written in the matrix form

$$\mathbf{F}(\cdot, \sigma) = K(\cdot, \sigma) * \mathbf{f},$$

where $\mathbf{f} = (f_1, f_2)^T, \mathbf{F} = (F_1, F_2)^T$; in Fourier representation

$$\widehat{\mathbf{F}}(\xi, \sigma) = \widehat{K}(\xi, \sigma)\widehat{\mathbf{f}}(\xi). \tag{2.21}$$

We assume grey-level shift invariance, rotational invariance and semi-group property (Sections 2.1.1, 2.1.2 and 2.1.4 respectively) and look for conditions on $K(\cdot, \sigma)$ to ensure scale invariance. The arguments can follow similar steps to those of [15]:

(A) *Dimensional analysis.* The application of the Pi-theorem (see e. g. [15] and references therein) to (2.21) leads to dimensionless variables $F_i/f_j, i, j = 1, 2$ and $\sigma\xi$ and dimension analysis provides the relations

$$\pi_{ij} = F_i f_j^{-1} \xi\sigma \approx 1,$$

in such a way that (2.21) can be written in the form

$$\widehat{\mathbf{F}}(\xi, \sigma) = \widetilde{K}(\xi\sigma)\widehat{\mathbf{f}}(\xi),$$

for some matrix $\widetilde{K} : \mathbb{R}^2 \to \mathbb{R}^2 \times \mathbb{R}^2$ with $\widetilde{K}(\mathbf{0}) = I$ (in order to have $\widehat{\mathbf{F}}(\xi, 0) = \widehat{\mathbf{f}}(\xi)$). Actually, rotational invariance implies that we can assume $\widetilde{K}(\xi\sigma) = \widetilde{K}(|\xi\sigma|)$ and write (2.21) as

$$\widehat{\mathbf{F}}(\xi, \sigma) = \widetilde{K}(|\xi\sigma|)\widehat{\mathbf{f}}(\xi), \tag{2.22}$$

for some $\widetilde{K} : \mathbb{R} \to \mathbb{R}^2 \times \mathbb{R}^2$ with $\widetilde{K}(0) = I$.

(B) *Scale invariance.* Now, semigroup condition (2.20) is, according to (2.22), of the form

$$\widetilde{K}(|\xi\sigma_1|)\widetilde{K}(|\xi\sigma_2|) = \widetilde{K}(|\xi\varphi^{-1}(\varphi(\sigma_1)+\varphi(\sigma_2))|), \tag{2.23}$$

for $\sigma_1, \sigma_2 \geq 0$. The same arguments as those in [15] can be used to show that scale invariance implies that φ in (2.19) must be of the form

$$\varphi(\sigma) = C\sigma^p,$$

for some constant $C > 0$ (which can be taken as $C = 1$) and $p > 0$. (In [17], p is identified as α.) Hence if $H(x^p) \equiv \widetilde{K}(x)$ then (2.23) reads

$$H(|\xi\sigma_1|^p)H(|\xi\sigma_2|^p) = H(|\xi\sigma_1|^p + |\xi\sigma_2|^p),$$

which is identified as the functional equation

$$\Psi(\alpha_1)\Psi(\alpha_1) = \Psi(\alpha_1+\alpha_2)$$

characterizing the matrix exponential function. Therefore $\widetilde{K}$ must be of the form

$$\widetilde{K}(|\xi\sigma|) = H(|\xi\sigma|^p) = e^{|\xi\sigma|^p A}, \quad p > 0$$

for some 2×2 real matrix A. Under hypotheses (H2), (H3) of Section 2.1.3, $\widetilde{K}$ must vanish at infinity (that is, each component of $\widehat{K}$ is in C_0); therefore

$$\widehat{K}(\xi,\sigma) = \widetilde{K}(|\xi\sigma|) = e^{-|\xi\sigma|^p d},$$

for some positive definite matrix d. In terms of the original scale t,

$$\widehat{K}(\xi,t) = e^{-t|\xi|^p d}, \quad p > 0. \tag{2.24}$$

Note that the case $p = 2$ corresponds to the kernel studied in the example 2. In particular, example 1 appears when

$$d = \begin{pmatrix} \alpha_R & -\alpha_I \\ \alpha_I & \alpha_R \end{pmatrix}, \quad \alpha_R > 0, \alpha_I \in \mathbb{R}.$$

(a)

(b)

(c)

FIGURE 14. (a) Noisy image with $\sigma = 35$; (b)-(e) Restored image at t_* with (1.1) and $\mathbf{u}_0 = \mathbf{u}_0^{(j)}$, $j = 3, 4$.

(a)

(b)

(c)

FIGURE 13. (a) Noisy image with $\sigma = 35$; (b)-(e) Restored image at t_* with (1.1) and $\mathbf{u}_0 = \mathbf{u}_0^{(j)}, j = 1, 2$.

2.1.6. *Infinitesimal generator.* Semigroup property can also be analyzed from the point of view of the infinitesimal generator. If $\mathbf{u}$ evolves like (2.3) with K_t satisfying (2.17), then its character can be determined from the spectrum and regularity of the infinitesimal generator (2.4), [18, 24]. The following example will illustrate this.

Example 3. *We may consider the linear complex filtering with D given by (2.8) on $X = H^1(\mathbb{R}^2) \times H^1(\mathbb{R}^2)$ and domain $\mathrm{Dom}(D) = H^2(\mathbb{R}^2) \times H^2(\mathbb{R}^2)$. Consider the eigenvalue problem for D:*

$$(\lambda I - D)\mathbf{u} = \mathbf{f}, \tag{2.25}$$

where I is the 2×2 identity matrix, $\mathbf{u} = (u, v)^T, \mathbf{f} = (f, g)^T$. In terms of the Fourier transform, (2.25) reads

$$\begin{aligned} (\lambda + \alpha_R|\xi|^2)\widehat{u}(\xi) - \alpha_I|\xi|^2\widehat{v}(\xi) &= \widehat{f}(\xi), \\ \alpha_I|\xi|^2\widehat{u}(\xi) + (\lambda + \alpha_R|\xi|^2)\widehat{v}(\xi) &= \widehat{g}(\xi), \end{aligned} \tag{2.26}$$

with $\xi = (\xi_1, \xi_2)^T, |\xi|^2 = \xi_1^2 + \xi_2^2$. Inverting (2.26) leads to

$$\begin{aligned} \widehat{u}(\xi) &= \frac{(\lambda + \alpha_R|\xi|^2)}{m(\xi)}\widehat{f}(\xi) + \frac{\alpha_I|\xi|^2}{m(\xi)}\widehat{g}(\xi), \\ \widehat{v}(\xi) &= -\frac{\alpha_I|\xi|^2}{m(\xi)}\widehat{f}(\xi) + \frac{(\lambda + \alpha_R|\xi|^2)}{m(\xi)}\widehat{g}(\xi), \\ m(\xi) &= (\lambda + \alpha_R|\xi|^2)^2 + (\alpha_I|\xi|^2)^2. \end{aligned}$$

Note now that since $\alpha_R > 0$, for any $\lambda > 0$ we have

$$\frac{(\lambda + \alpha_R|\xi|^2)}{m(\xi)} \leq \frac{1}{\lambda + \alpha_R|\xi|^2} \leq \frac{1}{\lambda},$$

and also, since

$$|\lambda + \alpha_R|\xi|^2||\alpha_I|\xi|^2| \leq \frac{m(\xi)}{2},$$

then

$$\frac{|\alpha_I|\xi|^2|}{m(\xi)} \leq \frac{1}{2(\lambda + \alpha_R|\xi|^2)} \leq \frac{1}{2\lambda}.$$

Therefore, Hille-Yosida Theorem, [4], implies that $D : X \to X$ in (2.8) with $\alpha_R > 0$ is the infinitesimal generator in X of a C_0-semigroup of contractions $K_t, t \geq 0$. The argument is valid when defining $D : X_k \to X_k$ being $X_k = H^k(\mathbb{R}^2) \times H^k(\mathbb{R}^2)$ and domain $\mathrm{Dom}(D) = X_{k+1}, k \geq 1$.

This approach can be generalized to kernels of the form (2.24) under the conditions of Section 2.1.5, where $\widehat{D}(\xi) = -|\xi|^p d, p > 0$.

2.1.7. *Locality.* A semigroup of operators $k_t, t \geq 0$ satisfies the locality condition if for all smooth f, g in its domain and all $\mathbf{x}$

$$(k_t f - k_t g)(\mathbf{x}) = o(t), \quad t \to 0^+,$$

whenever $D^{(n)} f(\mathbf{x}) = D^{(n)} g(\mathbf{x})$ for all $n \geq 0$. This means that for small t the value of $k_t f(\mathbf{x})$ is determined by the behaviour of f near $\mathbf{x}$. Mathematically, [1, 17], the locality property implies that the infinitesimal generator is a local differential operator.

In terms of the Fourier transform and the matrix kernels satisfying (2.24) we have

$$\left(\widehat{\frac{\mathcal{K}_h \mathbf{f} - \mathbf{f}}{h}}\right)(\xi) = \left(\frac{e^{-h|\xi|^p d} - I}{h}\right) \widehat{\mathbf{f}}(\xi).$$

If $h \to 0^+$ and inverting the Fourier transform, we would obtain a representation of the infinitesimal generator. Formally

$$\frac{e^{-h|\xi|^p d} - I}{h} = \sum_{j=1}^{\infty} \frac{(-1)^j h^{j-1} |\xi|^{jp}}{j!} d^j.$$

Therefore

$$\lim_{h \to 0^+} \frac{e^{-h|\xi|^p d} - I}{h} = -|\xi|^p d.$$

The limit would be the Fourier symbol of the operator, [18]

$$D\mathbf{f} = -(-\Delta)^{p/2} d\mathbf{f}, \tag{2.27}$$

with Δ the Laplace operator and where $(-\Delta)^{p/2}$ is multiplying each entry of d. Then (2.27) is local only for integer values of $p/2$ and the result obtained in [17] can be extended to this cross-diffusion case.

2.2. Generalized small theta approximation. One of the arguments to consider complex diffusion as an alternative for image processing is the so-called small theta approximation, [11]. This means that for small values of the imaginary part of the complex diffusion coefficient, the corresponding imaginary part of the solution of the evolutionary diffusion problem behaves in the limit as a scaled smoothed Gaussian derivative of the initial signal.

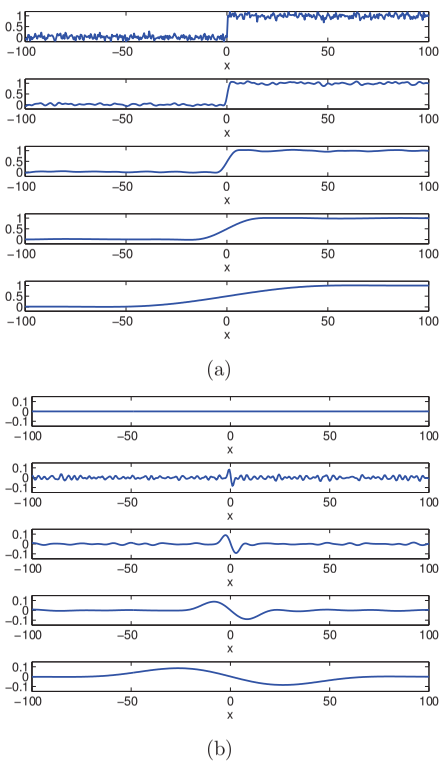

FIGURE 12. Cross-diffusion with $p = 2$ and for $d_{11} = d_{22} = 1, d_{12} = -0.9, d_{21} = 0.8$. Profiles of (a) u and (b) v at times $t_* = 0, 0.25, 2.5, 25, 250$. The initial data is a step pulse with Gaussian white noise of standard deviation $\sigma = 0.1$.

between the original S and the restored U images, computed as

$$r(S,U) = \frac{\sum_{i,j}(S_{ij} - \bar{S})(U_{ij} - \bar{U})}{\|S - \bar{S}\|_F \|U - \bar{U}\|_F}, \tag{3.3}$$

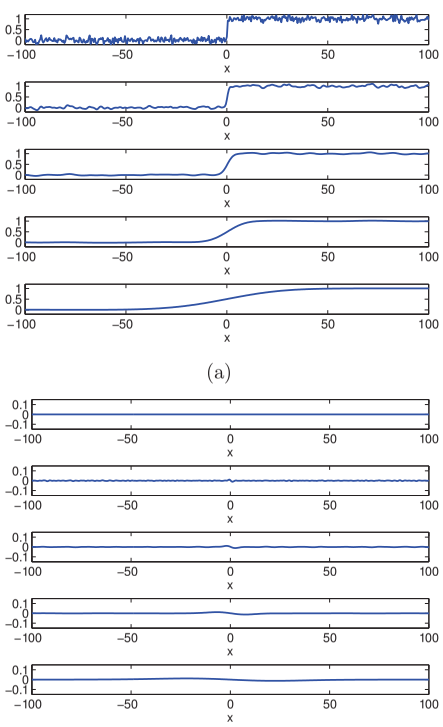

FIGURE 11. Cross-diffusion with $p = 2$ and for $d_{11} = d_{22} = 1, d_{12} = 0.2, d_{21} = 0.1$. Profiles of (a) u and (b) v at times $t_* = 0, 0.25, 2.5, 25, 250$. The initial data is a step pulse with Gaussian white noise of standard deviation $\sigma = 0.1$.

and linear complex diffusion ($d_{21} = -d_{12} = \mu, d_{11} = d_{22} = \nu > 0, \mathbf{u}_0 = (f, 0)^T$). To this end, an original image f was taken in the initial condition $\mathbf{u}_0 = (f, 0)^T$ in (2.3); this evolved according to (2.28) with different matrices d and using $p = 2$. (The results with other values of p have also been compared but will not be shown here.) The evolved image $\mathbf{u} = (u, v)^T$ is computed at values $t = 0.25, 2.5, 25$, as well as the corresponding correlation coefficient

This idea can also be discussed in the context of cross-diffusion systems (2.3), where D is the infinitesimal generator (2.27), that is

$$\mathbf{u}(\mathbf{x}, t) = e^{tD}\mathbf{u}_0(\mathbf{x}) = e^{-t(-\Delta)^{p/2}d}\mathbf{u}_0(\mathbf{x}). \tag{2.28}$$

If we decompose

$$d = a + b = \begin{pmatrix} d_{11} & 0 \\ 0 & d_{22} \end{pmatrix} + \begin{pmatrix} 0 & d_{12} \\ d_{21} & 0 \end{pmatrix},$$

then note that a and b commute if and only if

$$d_{11} = d_{22}. \tag{2.29}$$

Assume first that (2.29) holds and denote $\nu = d_{11} = d_{22} > 0$. We may analyze the behaviour of (2.28) by using this property, since now we can write

$$\begin{aligned} e^{tD} &= e^{-ta(-\Delta)^{p/2}} e^{-tb(-\Delta)^{p/2}} \\ &= e^{-tb(-\Delta)^{p/2}} \begin{pmatrix} e^{-\nu t(-\Delta)^{p/2}} & 0 \\ 0 & e^{-\nu t(-\Delta)^{p/2}} \end{pmatrix} \end{aligned}$$

Then

$$\mathbf{u}(\mathbf{x}, t) = e^{-tb(-\Delta)^{p/2}} \begin{pmatrix} e^{-\nu t(-\Delta)^{p/2}} u_0(\mathbf{x}) \\ e^{-\nu t(-\Delta)^{p/2}} v_0(\mathbf{x}) \end{pmatrix}. \tag{2.30}$$

We now study the first matrix exponential. Due to the form of b we have

$$b^{2m} = (d_{12}d_{21})^m I, \quad b^{2m+1} = (d_{12}d_{21})^m b, \ m = 0, 1, \ldots,$$

where I stands for the 2×2 identity matrix. Therefore we can formally write, [24]

$$\begin{aligned} e^{-tb(-\Delta)^{p/2}} &= \sum_{m=0}^{\infty} \frac{(-t)^{2m}}{2m!} (-\Delta)^{\frac{2mp}{2}} (d_{12}d_{21})^m I \\ &\quad + \sum_{m=0}^{\infty} \frac{(-t)^{2m+1}}{(2m+1)!} (-\Delta)^{\frac{(2m+1)p}{2}} (d_{12}d_{21})^m b. \end{aligned} \tag{2.31}$$

By defining the operator $A := -(-\Delta)^{p/2}$ and according to the sign of $d_{12}d_{21}$, the following cases hold:

(1) $d_{12}d_{21} > 0$. If $\mu := \sqrt{d_{12}d_{21}}$ then we can write $(d_{12}d_{21})^m = \mu^{2m} = \frac{1}{\mu}\mu^{2m+1}$ and (2.31) becomes the formal matrix operator (see [18])

$$e^{tbA} = \begin{pmatrix} \cosh(t\mu A) & \frac{d_{12}}{\mu}\sinh(t\mu A) \\ \frac{d_{21}}{\mu}\sinh(t\mu A) & \cosh(t\mu A) \end{pmatrix},$$

where the hyperbolic cosine and sine of the operator are defined in the standard way from the exponential, [24]. Then if μ is small

$$e^{tbA} \approx I + tbA, \tag{2.32}$$

and (2.30) can be approximated by

$$\begin{aligned} \mathbf{u}(\mathbf{x},t) &\approx (I + tbA)\begin{pmatrix} e^{\nu tA}u_0(\mathbf{x}) \\ e^{\nu tA}v_0(\mathbf{x}) \end{pmatrix} \\ &= \begin{pmatrix} e^{\nu tA}u_0(\mathbf{x}) + td_{12}A\left(e^{\nu tA}v_0(\mathbf{x})\right) \\ td_{21}A\left(e^{\nu tA}u_0(\mathbf{x})\right) + e^{\nu tA}v_0(\mathbf{x}) \end{pmatrix}. \end{aligned} \tag{2.33}$$

Formula (2.33) generalizes the small theta approximation emphasized in [11] in the following sense. Given $f \in L^1(\mathbb{R}^2)$ if d_{21} is small we may take $\mathbf{u}_0 = (f, 0)^T$ and then

$$\mathbf{u}(\mathbf{x},t) = \begin{pmatrix} u(\mathbf{x},t) \\ v(\mathbf{x},t) \end{pmatrix} \approx \begin{pmatrix} e^{\nu tA}f(\mathbf{x}) \\ td_{21}A\left(e^{\nu tA}f(\mathbf{x})\right) \end{pmatrix}.$$

Thus $v(\mathbf{x},t)$ satisfies

$$\lim_{d_{21}\to 0}\frac{v(\mathbf{x},t)}{d_{21}} = tA\left(e^{\nu tA}f(\mathbf{x})\right).$$

If d_{12} is small, we may take $\mathbf{u}_0 = (0, f)^T$ and then

$$\mathbf{u}(\mathbf{x},t) = \begin{pmatrix} u(\mathbf{x},t) \\ v(\mathbf{x},t) \end{pmatrix} \approx \begin{pmatrix} td_{12}A\left(e^{\nu tA}f(\mathbf{x})\right) \\ e^{\nu tA}f(\mathbf{x}) \end{pmatrix}.$$

Thus $u(\mathbf{x},t)$ satisfies

$$\lim_{d_{12}\to 0}\frac{f(\mathbf{x},t)}{d_{12}} = tA\left(e^{\nu tA}f(\mathbf{x})\right).$$

(2) The discussion of the cases $d_{12} = 0, d_{21} \neq 0$ and $d_{21} = 0, d_{21} \neq 0$ is similar. In both the matrix b is triangular and $b^2 = 0$; therefore (2.32)

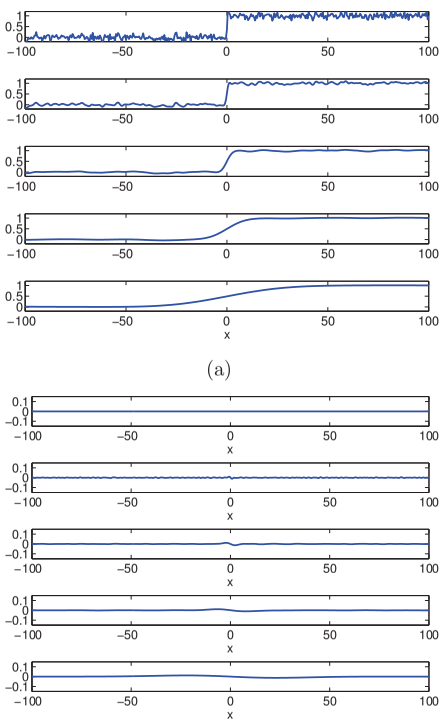

FIGURE 10. Cross-diffusion with $p = 2$ and for $d_{11} = d_{22} = 1, d_{12} = -0.1, d_{21} = 0.1$. Profiles of (a) u and (b) v at times $t_* = 0, 0.25, 2.5, 25, 250$. The initial data is a step pulse with Gaussian white noise of standard deviation $\sigma = 0.1$.

not look to make influence in the quality of restoration. This behaviour with respect to p was also observed when using the rest of the computed initial data.

3.2.3. *Some comparisons with linear real and complex diffusion.* A final experiment attempts to compare the blurring effect of some examples of linear cross-diffusion systems with those given by the particular cases of Gaussian smoothing (obtained with $d_{12} = d_{21} = 0, d_{11} = d_{22} = \nu > 0$ and $\mathbf{u}_0 = (f, 0)^T$)

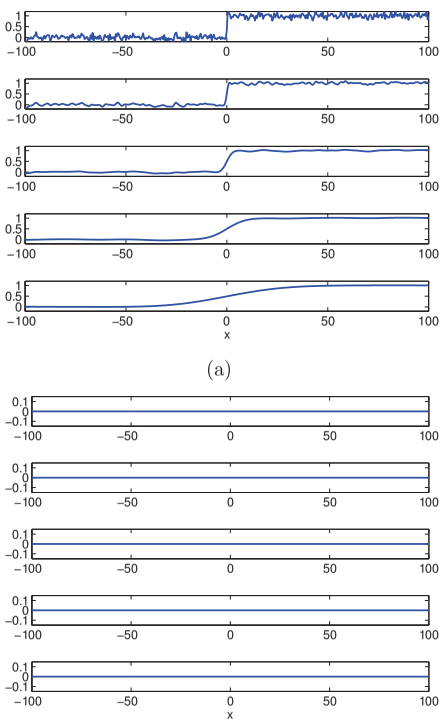

(a)

(b)

FIGURE 9. Cross-diffusion with $p = 2$ and for $d_{11} = d_{22} = 1, d_{12} = d_{21} = 0$. Profiles of (a) u and (b) v at times $t_* = 0, 0.25, 2.5, 25, 250$. The initial data is a step pulse with Gaussian white noise of standard deviation $\sigma = 0.1$.

checked by taking a different type of noise, namely a uniformly distributed white noise with the same values of σ as above.

3.2.2. *Choice of p.* A second point is related to the influence of the local character of the infinitesimal generator (2.27) on the quality of filtering. This is studied by comparing the SNR and $PSNR$ indexes obtained with several values of p from a noisy image and at final time $t_* = 2$. Figure 16 shows that the SNR and $PSNR$ values increase with p. In this sense, locality does

is actually an equality. Thus, (2.33) becomes

$$\begin{aligned}\mathbf{u}(\mathbf{x},t) &= (I+tbA)\begin{pmatrix}e^{\nu tA}u_0(\mathbf{x})\\ e^{\nu tA}v_0(\mathbf{x})\end{pmatrix}\\ &= \begin{pmatrix}e^{\nu tA}u_0(\mathbf{x})\\ td_{21}A\left(e^{\nu tA}u_0(\mathbf{x})\right)+e^{\nu tA}v_0(\mathbf{x})\end{pmatrix},\end{aligned}$$

in the first case and

$$\begin{aligned}\mathbf{u}(\mathbf{x},t) &= (I+tbA)\begin{pmatrix}e^{\nu tA}u_0(\mathbf{x})\\ e^{\nu tA}v_0(\mathbf{x})\end{pmatrix}\\ &= \begin{pmatrix}e^{\nu tA}u_0(\mathbf{x})+td_{12}A\left(e^{\nu tA}v_0(\mathbf{x})\right)\\ e^{\nu tA}v_0(\mathbf{x})\end{pmatrix},\end{aligned}$$

in the second one. Then a generalization of the small theta approximation property can also be derived as before.

(3) $d_{12}d_{21} < 0$. If $\mu := \pm\sqrt{-d_{12}d_{21}}$ then we can write $(d_{12}d_{21})^m = (-1)^m\mu^{2m} = \frac{(-1)^m}{\mu}\mu^{2m+1}$ and now (2.31) becomes

$$e^{tbA} = \begin{pmatrix}\cos(t\mu A) & \frac{d_{12}}{\mu}\sin(t\mu A)\\ \frac{d_{21}}{\mu}\sin(t\mu A) & \cos(t\mu A)\end{pmatrix},$$

where the cosine and sine functions are also defined from the exponential function. Then again if μ is small (2.32) holds, and (2.30) can be approximated as before, using (2.33), generalizing the small theta approximation in a similar way. Actually, this small theta approximation appears as particular case when $d_{12} = -d_{21}$ taking for instance $\mu = |d_{21}|\sin\theta$ for some $\theta \in (-\pi/2, \pi/2)$, [11].

The case $d_{11} \neq d_{22}$ cannot be treated as before since the matrices a and b do not commute anymore. Instead, we may use the eigenvalues (2.10) of d, written in the form

$$\lambda_\pm = \frac{1}{2}\left(\nu \pm \sqrt{\delta}\right),$$
$$\nu = d_{11}+d_{22}, \quad \delta = (d_{11}-d_{22})^2 + 4d_{12}d_{21}.$$

Similar conclusions to those above are obtained when discussing the behaviour of solutions (2.30) in terms of the sign of δ and using the reformulation given by a basis of eigenvectors.

3. Numerical experiments

This section is devoted to illustrate numerically the behaviour of linear filters of cross-diffusion. Here the purpose is two-fold. First, the dependence of the models on some parameters, such as the initial data $\mathbf{u}_0$, the matrix d and the power p of (2.27), motivates a discussion, by computational means, about their influence on the performance of the restoration process. The second purpose is to compare this performance with different filters. Especial attention will be paid to this comparison when Gaussian smoothing and linear complex diffusion, considered as particular cases of cross-diffusion formulation, are involved.

Several numerical experiments for one- and two-dimensional signals are carried out. In all of them, the computations are made with Fourier techniques, [5]. Specifically, for the case in one dimension, an interval $(-L, L)$ with large L is defined and discretized by Fourier collocation points $x_j = -L + jh, j = 0, \ldots, N$, with stepsize h and the signal is represented by the corresponding interpolant trigonometric polynomial with the coefficients computed by the DFT of the signal values at the collocation points. For experiments with images, the implementation follows the corresponding Fourier techniques in two dimensions, with discretized intervals $(-L_x, L_x)\times(-L_y, L_y), L_x, L_y$ large, by Fourier collocation points (x_j, y_k), with $x_j = -L_x + jh_x, j = 0, \ldots, N_x$, $y_k = -L_y + kh_y, k = 0, \ldots, N_y$, and the image is represented by the interpolant trigonometric polynomial at the collocation points, computed with the two-dimensional version of the DFT. In both cases, from the Fourier representation, the convolution (1.1) is implemented in the Fourier space by using (2.24).

3.1. Experiments in 1D. The evolution of a one-dimensional signal f (a unit-step function), clean and noisy, with kernels of symbols (2.27) and initial condition $\mathbf{u}_0 = (f, 0)^T$ is first studied. We start with the clean signal. The main conclusions suggested by the numerical experiments (see Figures 1-8) are the following:

(1) The first component is affected by a smoothing effect. This is stronger as d_{11}, d_{22} which, by (2.9), have to be positive, and $|d_{12}|, |d_{21}|$ grow.
(2) Except in the Gaussian smoothing case ($d_{12} = d_{21} = 0$), the second component develops a sort of small-amplitude Gaussian derivative-type monopulse. Again, the height of the amplitude looks to depend on how large (in absolute value) the elements of d are, with the larger

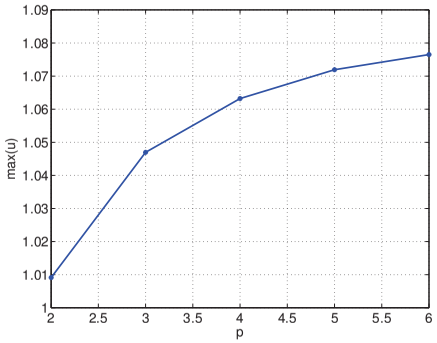

FIGURE 8. Cross-diffusion for $d_{11} = d_{22} = 1, d_{12} = -0.9, d_{21} = 0.8$. Maximum of u vs. p at time $t_* = 2.5$.

TABLE 2. SNR (top) and $PSNR$ (bottom) values at $t_* = 1$.

σ	15	25	35	45
$\mathbf{u}_0^{(1)}$	11.02	10.63	10.01	9.27
$\mathbf{u}_0^{(2)}$	10.87	10.52	9.97	9.22
$\mathbf{u}_0^{(3)}$	11.01	10.60	10.04	9.28
$\mathbf{u}_0^{(4)}$	11.32	10.84	10.15	9.43
σ	15	25	35	45
$\mathbf{u}_0^{(1)}$	25.66	25.21	24.58	23.87
$\mathbf{u}_0^{(2)}$	25.50	25.09	24.50	23.82
$\mathbf{u}_0^{(3)}$	25.67	25.20	24.57	23.87
$\mathbf{u}_0^{(4)}$	25.99	25.41	24.70	23.94

Figure 15 shows the evolution of the SNR (Figure (a)) and $PSNR$ (Figure (b)) parameters with t_* when considering $\mathbf{u}_0^{(1)}$ and $\mathbf{u}_0^{(4)}$ as initial data and from an additive Gaussian noise with $\sigma = 30$. Both parameters attain a maximum value from which the quality of restoration is deteriorated by the blurring effect. These maximum values are larger in the case of $\mathbf{u}_0^{(1)}$ but from $\mathbf{u}_0^{(4)}$ the time evolution looks to behave better. This relative equivalence of results using different initial decomposition of the noisy image was also

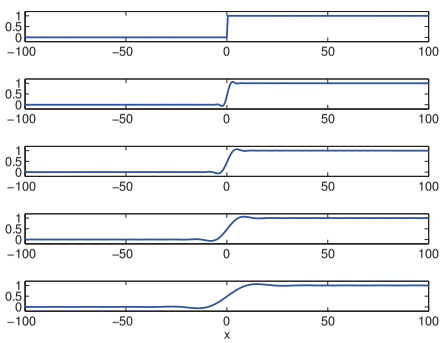

(a)

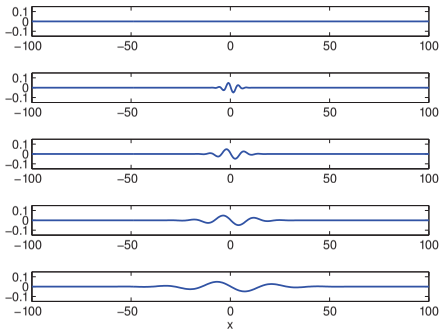

(b)

FIGURE 7. Cross-diffusion with $p = 4$ and for $d_{11} = d_{22} = 1, d_{12} = -0.9, d_{21} = 0.8$. Profiles of (a) u and (b) v at times $t_* = 0, 0.25, 2.5, 25, 250$.

The results are shown in Table 2. The values of $\mathbf{u}_0$ for the experiments are

$$\mathbf{u}_0^{(1)} = (f, 0)^T, \mathbf{u}_0^{(2)} = (f, \Delta f)^T,$$
$$\mathbf{u}_0^{(3)} = (f, |\nabla f|)^T, \mathbf{u}_0^{(4)} = (f, -|\nabla f|\Delta f)^T.$$

The final time is $t_* = 1$. The restored images corresponding to $\sigma = 35$ are displayed in Figures 13, 14. In view of Table 2, it may be worth mentioning the slightly better behaviour of $\mathbf{u}_0^{(4)}$. Both SNR and $PSNR$ values also vary with the final time t_* where the process stops at. By way of illustration,

the parameters the taller the wave is. In particular, this property may illustrate the effect of the small theta approximation in complex diffusion (Figure 2) and in more general cross-diffusion models (Figures 3-5). In this sense, no relevant differences appear to be observed when considering different signs of d_{12} and d_{21}.

(3) The influence of the values of p is illustrated in Figures 5-7. Note that as p grows the first component develops small oscillations at the points with less regularity. On the other hand, the second component increases somehow the number of pulses. Figure 8 shows that the maximum of the first component is growing with p.

The impression that the models are relatively equivalent as filters is enforced when the unit step is affected by some noise and the evolution of the noisy signal, taken as initial condition, is monitored. This is illustrated by the following experiments, where a Gaussian-type white noise is taken. Some points can be emphasized (see Figures 9-12):

(1) In all the cases considered, the evolution filters the signal in a process that mainly depends on d_{11}, d_{22}. The blurring effect looks however attenuated a bit when the small theta approximation (with linear complex diffusion or more general cross-diffusion with small in magnitude non-diagonal entries) is present.

(2) Table 1 displays several parameters to measure the noise of a signal and therefore they evaluate somehow the quality of denoising at different times. They are:

- Root-Mean-Square-Error (RMSE):

$$RMSE(f, g) = \frac{1}{\sqrt{l}}||f - g||_2.$$

- Signal-to-Noise-Ratio (SNR):

$$SNR(f, g) = 10 \log_{10} \left(\frac{\text{var}(g)}{\text{var}(f - g)} \right). \tag{3.1}$$

- Peak Signal-to-Noise-Ratio (PSNR):

$$\begin{aligned} PSNR(f, g) &= 10 \log_{10} \left(\frac{l^2}{||f - g||_2^2} \right) \\ &= 20 \log_{10} \left(\frac{l}{RMSE(f, g)} \right), \end{aligned} \tag{3.2}$$

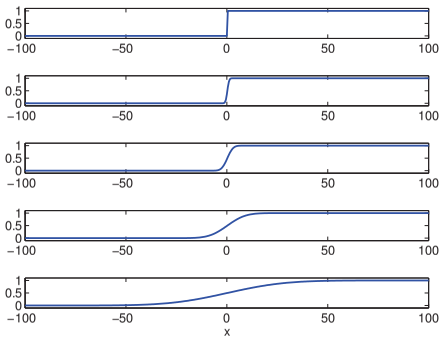

(a)

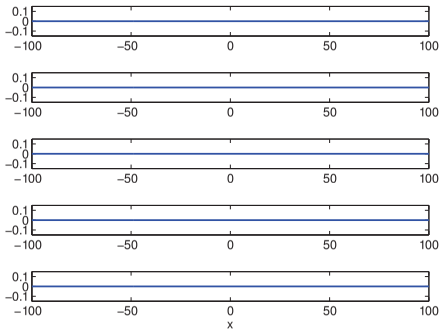

(b)

FIGURE 1. Cross-diffusion with $p = 2$ and for $d_{11} = d_{22} = 1, d_{12} = d_{21} = 0$. Profiles of (a) u and (b) v at times $t_* = 0, 0.25, 2.5, 25, 250$.

where f and g are, respectively, the original and restored signals, l is their length and $\mathrm{var}(x)$ is the variance of the vector x.

The computations correspond to filter a noisy unit step pulse with Gaussian white noise of standard deviation $\sigma = 0.1$. The choices of d are as follows: in all the cases $d_{11} = d_{22} = 1$ and

(C1) $d_{12} = d_{21} = 0$ (Gaussian smoothing).
(C2) $d_{12} = -\mu, d_{21} = \mu, \mu = 0.1$. (Linear complex diffusion.)
(C3) $d_{12} = -\mu, d_{21} = \mu, \mu = 1$. (Linear complex diffusion.)

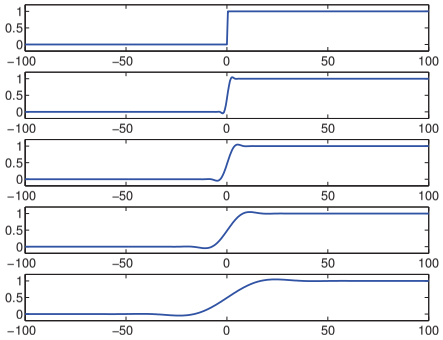

(a)

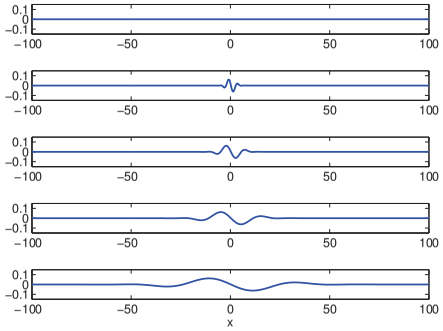

(b)

FIGURE 6. Cross-diffusion with $p = 3$ and for $d_{11} = d_{22} = 1, d_{12} = -0.9, d_{21} = 0.8$. Profiles of (a) u and (b) v at times $t_* = 0, 0.25, 2.5, 25, 250$.

by using (2.1). For each $\mathbf{u}_0$ and all the noisy images, the corresponding SNR and $PSNR$ values are calculated and compared to those given by the original image. In this case the computations formulas (3.1) and (3.2) are applied, where in this case f and g are, respectively, the original and restored image, $l = 255$ and the Euclidean norm in (3.2) is substituted by the Frobenius norm (divided by the corresponding factor of the dimension of the matrices).

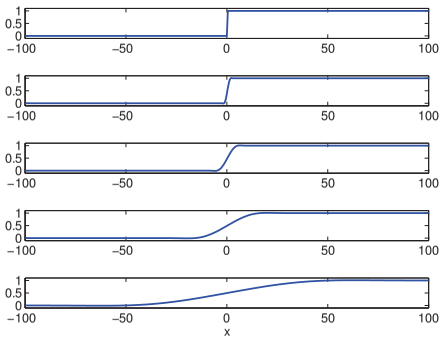

(a)

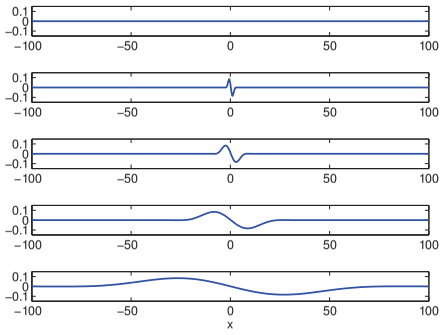

(b)

FIGURE 5. Cross-diffusion with $p = 2$ and for $d_{11} = d_{22} = 1, d_{12} = -0.9, d_{21} = 0.8$. Profiles of (a) u and (b) v at times $t_* = 0, 0.25, 2.5, 25, 250$.

the required conditions (2.9), namely

$$d = \begin{pmatrix} 1 & -0.1 \\ 0.01 & 1 \end{pmatrix}.$$

We also fix $p = 2$ and a suitable final time t_* which depends on the degradation of the image due to noise. We first take four noisy images from an ideal one by adding Gaussian white noise with standard deviation $\sigma = 15, 25, 35, 45$. For several choices of $\mathbf{u}_0$ the evolved image $\mathbf{u}$ at t_* is computed

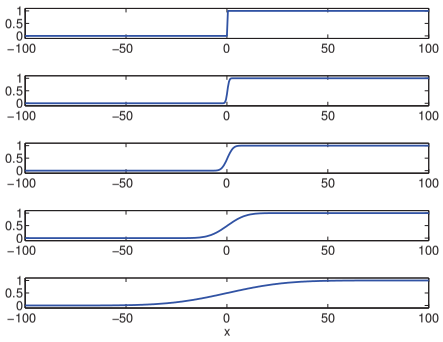

(a)

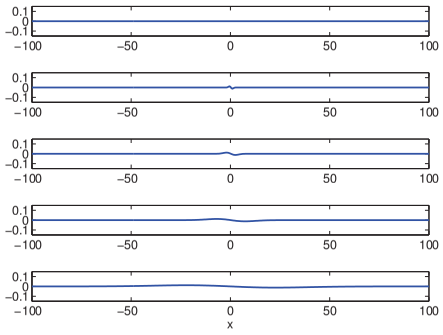

(b)

FIGURE 2. Cross-diffusion with $p = 2$ and for $d_{11} = d_{22} = 1, d_{12} = -0.1, d_{21} = 0.1$. Profiles of (a) u and (b) v at times $t_* = 0, 0.25, 2.5, 25, 250$.

(C4) $d_{12} = 0.2, d_{21} = 0.1$.
(C5) $d_{12} = -0.9, d_{21} = 0.8$.

Note that the best values at $t_* = 0.25$ are given by (C3) while for longer times ($t_* = 2.5, 25$, the first one is not shown in the table) we need to make use of the small theta approximation, with smaller values of d_{12}, d_{21}; thus (C4) behaves better. (Since $RMSE$ compares the original and the denoised signals, it is measuring how close the signals are and, consequently, the smaller the $RMSE$ the better the filtering is. On the contrary, larger SNR and $PSNR$

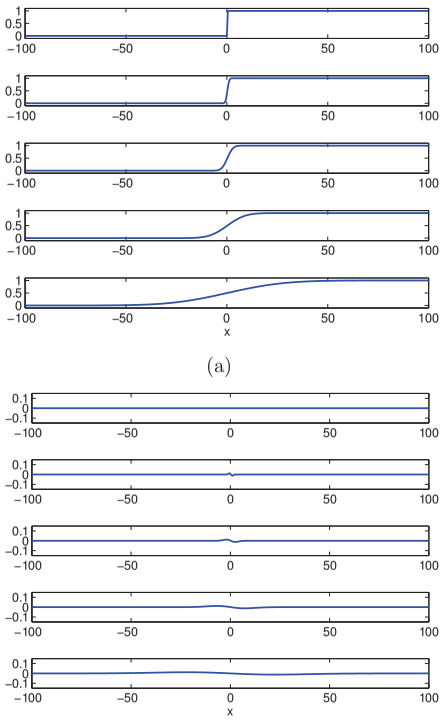

(a)

(b)

FIGURE 3. Cross-diffusion with $p = 2$ and for $d_{11} = d_{22} = 1, d_{12} = 0.2, d_{21} = 0.1$. Profiles of (a) u and (b) v at times $t_* = 0, 0.25, 2.5, 25, 250$.

values correspond to a smaller influence of the noise.) We finally note that larger values of σ give similar results.

3.2. Experiments in 2D.

3.2.1. *Choice of the initial data.* The numerical experiments presented here with two-dimensional images deal first with the choice of the components of the initial vector image $\mathbf{u}_0$. To this end, we consider a matrix d satisfying

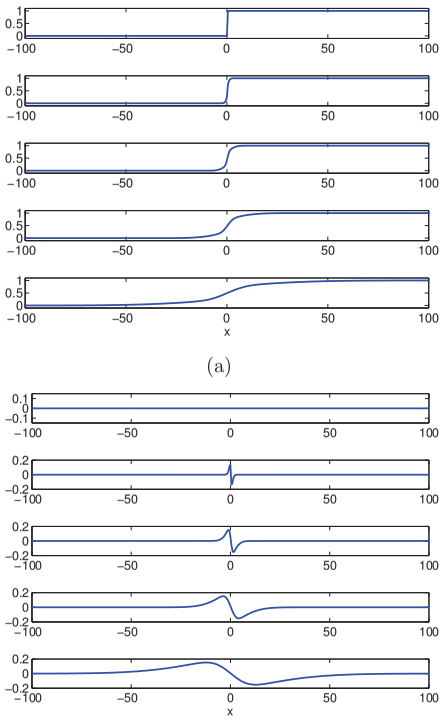

(a)

(b)

FIGURE 4. Cross-diffusion with $p = 2$ and for $d_{11} = d_{22} = 1, d_{12} = 0.9, d_{21} = 0.9$. Profiles of (a) u and (b) v at times $t_* = 0, 0.25, 2.5, 25, 250$.

TABLE 1. $RMSE$, SNR and $PSNR$ values. Gaussian white noise with $\sigma = 0.1$.

d	$t_* = 0.25$			$t_* = 25$		
	$RMSE$	SNR	$PSNR$	$RMSE$	SNR	$PSNR$
$(C1)$	$5.38E{-}2$	19.41	26.59	$8.07E{-}2$	15.58	22.09
$(C2)$	$5.38E{-}2$	19.41	26.59	$8.08E{-}2$	15.57	22.08
$(C3)$	$5.28E{-}2$	19.57	26.71	$8.67E{-}2$	14.74	21.24
$(C4)$	$5.38E{-}2$	19.40	26.58	$8.05E{-}2$	15.60	22.12
$(C5)$	$5.29E{-}2$	19.55	26.71	$8.68E{-}2$	14.93	21.43